Icarus **148**, 211–225 (2000)
doi:10.1006/icar.2000.6486, available online at http://www.idealibrary.com on IDEAL®

Silicate Cooling Model Fits to Galileo NIMS Data of Volcanism on Io

Ashley Gerard Davies, Rosaly Lopes-Gautier, William D. Smythe, and Robert W. Carlson

Jet Propulsion Laboratory—California Institute of Technology, 4800 Oak Grove Drive, Pasadena, California 91109-8099
E-mail: Ashley.Davies@jpl.nasa.gov

Received May 26, 1998; revised July 17, 2000

The Near Infrared Mapping Spectrometer (NIMS) has obtained spectra of volcanoes on the surface of the jovian satellite Io. Fits to data using a silicate cooling model allow us to constrain lava eruption rates and eruption age. The thermal signatures of the hot spots are indicative of active and cooling silicate lava flows. For large, active hot spots maximum ages of flow surfaces detected by NIMS typically range from days to months, although in one case it is nearly 30 years. Mass eruption rates for the main hot spots are in the range 7 m^3 s^{-1} to 79 m^3 s^{-1}, using an average flow thickness of 1 m. These mass eruption rates are orders of magnitude less than those implied for large thermal outbursts on Io: the eruptions observed during June 1996 are most likely of a different eruption style, on a much smaller scale. The observation analyzed here may be representative of the current background level of volcanic activity on the anti-jove hemisphere of Io. The global mass eruption rate from these "non-outburst" hot spots is calculated to be 43 km^3/year, equivalent to a global resurfacing rate of about 1 mm/year, about 10% of the minimum required global resurfacing volume. The total observed energy output from the 14 hot spots analyzed is 3.6×10^{12} W. Normalized globally, these hot spots contribute approximately 10% of Io's radiometric heat flux.

Key Words: **Io; volcanism; thermal; modeling.**

1. INTRODUCTION

The arrival at Jupiter of the Galileo spacecraft has resulted in observations in the infrared, at higher spatial resolution than ever seen before, of the volcanic forces that dominate Io, adding to the body of observations stretching back to the observation of an intense brightening (Witteborn *et al.* 1979) that was subsequently recognized as being of volcanic origin. A prediction of active volcanism driven by tidal heating (Peale *et al.* 1979) was spectacularly fulfilled when the Voyager spacecraft discovered a surface covered with volcanic landforms and detected nine volcanic plumes (Strom *et al.* 1981). The Infrared Interferometer Spectrometer (IRIS) on Voyager detected 22 volcanic hot spots (mostly linked to low-albedo features on the surface; see Smith *et al.* 1979, Pearl and Sinton 1982), having imaged approximately one-third of the surface of Io (Pearl and Sinton 1982, McEwen *et al.* 1992).

The composition of the material being erupted on the surface of Io has long been a subject of debate. Arguments have been made for both high-temperature silicate and lower temperature sulfur-dominated volcanism being the dominant volcanic process on Io. Bolstering the case for sulfur-dominated volcanism, the surface of Io is covered with sulfur dioxide and other sulfurous compounds (Smythe *et al.* 1979, Nash *et al.* 1986) and the variegated colors of the ionian surface have been likened to allotropes of sulfur (Sagan 1979, Soderblom *et al.* 1980, Pieri *et al.* 1984). Additionally, Io is the source of sulfur, oxygen, and sodium ions in the Io torus. On the other hand, favoring silicate volcanism, the bulk density of Io (3.57 g/cm^3) suggests a dominantly silicate composition, and Carr (1986) showed that a sulfur-dominated crust had insufficient strength to produce observed caldera morphologies. The highest IRIS-derived hot spot temperature was 654 K at Pele Patera, the site of a major volcanic plume, by Pearl and Sinton (1982) who noted that this was a non-unique solution and that temperatures as high as 854 K could be accommodated within the noise of the data. Carr argued that the observed topography, at least in the vicinity of Pele, had to be dominated by silicates as sulfur would be molten at 654 K.

The IRIS-derived temperatures failed to directly resolve the question of whether volcanism on Io was dominated by silicates, with temperatures from 900 K to greater than 1900 K, or by sulfur (390 to 600 K, perhaps up to 1000 K if sulfides are involved). Since Voyager and before Galileo, Earth-based observations have yielded color temperatures indicative of silicate volcanism (e.g., 1550 K in 1986; 1225 K in 1990 (Veeder *et al.* 1994, Blaney *et al.* 1995), 1200–1600 K (Davies 1996)). During the Galileo epoch, in the latter stages of 1996, high-temperature events were observed from groundbased instruments with temperatures in excess of 1400 K and with a minimum temperature of approximately 900 K (Stansberry *et al.* 1997, Spencer *et al.* 1997). These measurements greatly strengthened the case for a preponderance of silicate volcanism on Io (Carr 1986, Johnson *et al.* 1988, Blaney *et al.* 1995, Davies 1996). Additionally, multispectral observations of occultations of Io by other Galilean satellites have led to determination of some hot spot positions, areas and temperatures, especially on the jovian-facing hemisphere of Io (poorly imaged by Galileo-based instruments) to a high degree of accuracy (Howell *et al.* 1998, Goguen *et al.* 1998). Some occultation data have been fitted with the silicate flow model of Howell (1997), producing magma temperatures

0019-1035/00 $35.00

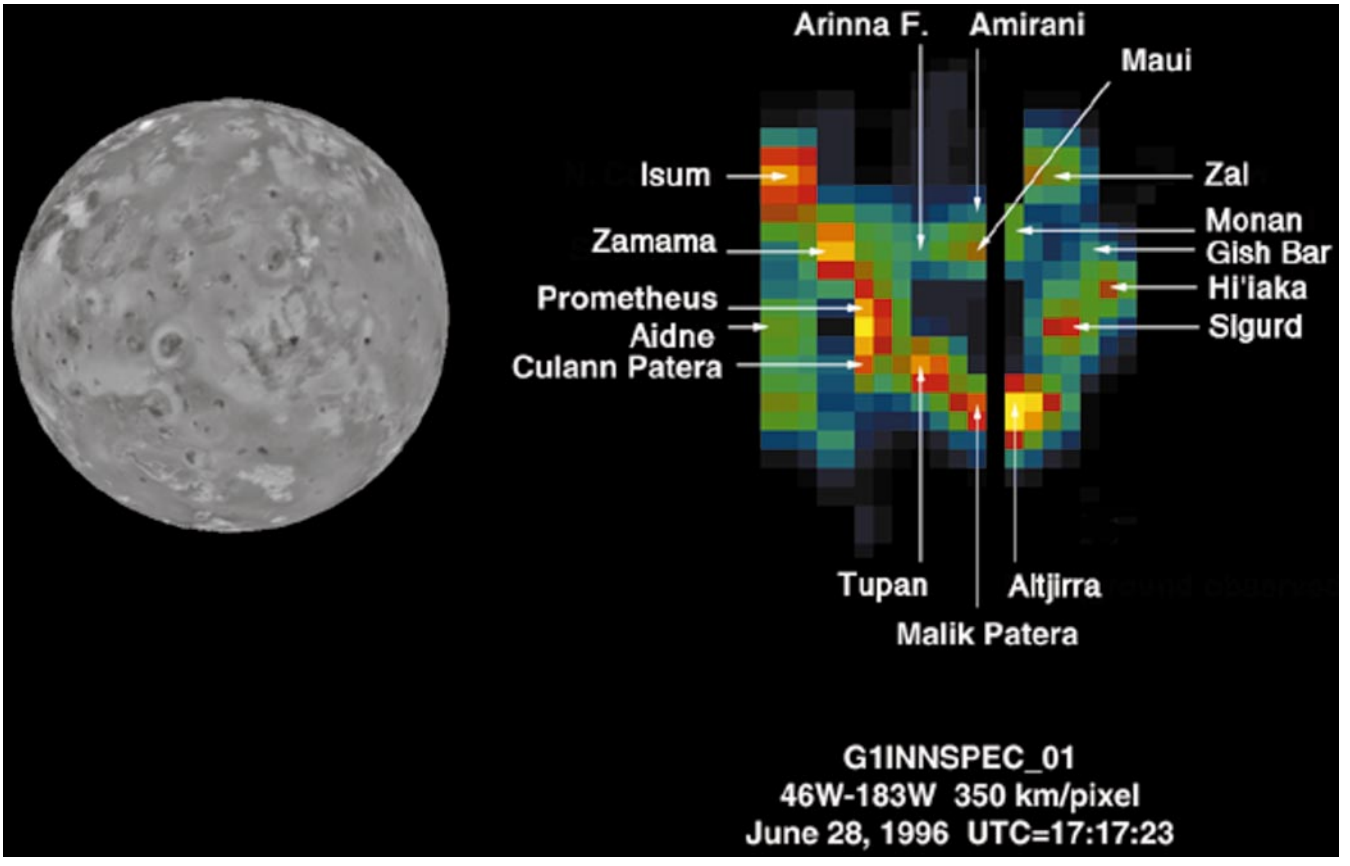

FIG. 1. NIMS Io observation G1INNSPEC01 obtained on 26 June 1996, 17:17 UT, during orbit G1. This observation has the instrument maximum of 408 wavelengths between 0.7 and 5.2 μm, although some wavelengths are lost to boom hits and radiation spikes. The figure shows Io at 4.9 μm covering longitudes in darkness from 46 W to 183 W. The major hot spots are labeled. Isum and Aidne are not included in the analysis in this paper as they are in the sunlit portion of Io. The sub-spacecraft point is 136 W, 5 N, and has a sub-spacecraft resolution of 350 km/pixel.

consistent with silicate volcanism (Spencer *et al.* 1997). Although silicate volcanism is apparently the dominant process for transfer of heat from the interior of Io to the surface, it is noted that interactions with abundant deposits of sulfur and sulfur-rich volatiles close to and on the surface will lead to secondary volcanic activity, including the formation of sulfur flows and large SO_2-rich volcanic plumes.

Fits to two-filter SSI eclipse and NIMS dark-side spectra from later orbits revealed components of the surface volcanics at temperatures typically in the range 1200–1600 K (McEwen *et al.* 1998a,b) with some cases, most notably at Pillan Patera, in the range 1700–2000 K. A case has been made for high-temperature sulfide volcanism on Io (Nash 1993) but the high density of this material would make surface eruption difficult (Keszthelyi and McEwen 1997a). The temperatures derived from SSI observations, well in excess of sulfur liquidus temperatures, indicate that the dominating volcanic process contributing to thermal emission at short infrared wavelengths from the hot spots is silicate in nature. In this paper we present the results of fitting a silicate lava-cooling model to the hot spot spectra obtained by NIMS during orbit G1.

2. GALILEO OBSERVES IO: ORBIT G1

The Galileo spacecraft entered into orbit around Jupiter on December 7th, 1995, and since June 1996 has been observing Io on nearly every orbit (Smythe *et al.* 1995): indeed, one of the primary mission tasks was the observation and monitoring of volcanism on Io. Accordingly, on 28 June 1996 at 17:17 UT, the Near Infrared Mapping Spectrometer (NIMS) on Galileo made one observation (G1INNSPEC01: see Fig. 1) from a range of 700,750 km. This provided a resolution of approximately 350 km per pixel at the sub-spacecraft point at 136 W, 5 N. This observation covered all latitudes and longitudes from 46 W to 190 W, covering most of the leading hemisphere and some of the anti-jovian hemisphere. Most of the observed area was in darkness, which meant that the hot spot spectra were for the most part uncontaminated by sunlight, simplifying analysis of the data. Ten hours later, on 29 June, Io was again observed, this time in eclipse, by the Solid State Imaging (SSI) experiment (Belton *et al.* 1996, McEwen *et al.* 1997). SSI is described in Belton *et al.* (1992). This observation covered all latitudes and longitudes from 150 W to 330 W. The observation revealed

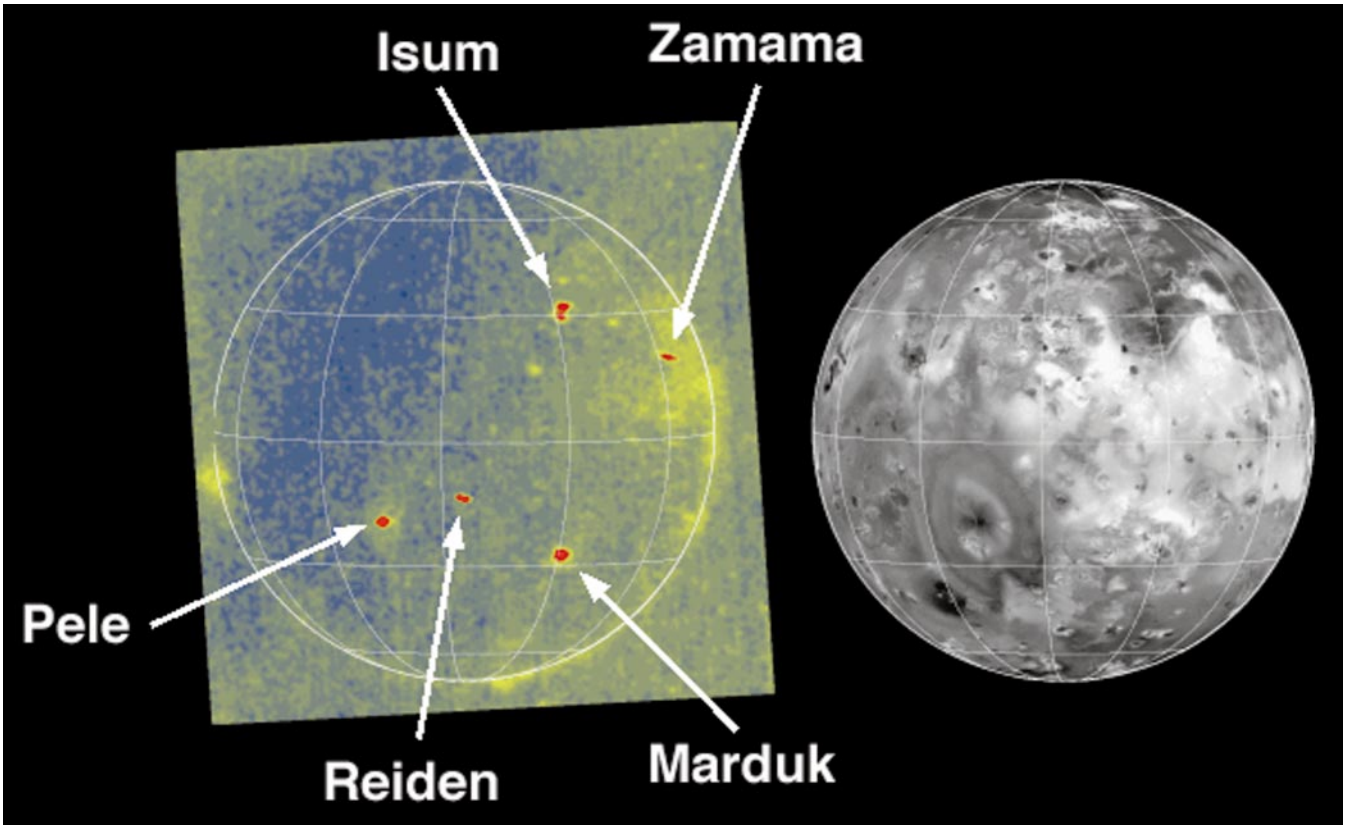

FIG. 2. SSI eclipse observation of Io G1ISIOECLI02 obtained on 29 June 1996, 03:47 UT. This is a clear filter image at an effective wavelength of 644 nm and a bandpass width of 440 nm. The glowing hot spots are (from right to left) Zamama, Isum (upper), Marduk (lower), Reiden Patera, and Pele. The sub-spacecraft point is at 235 W, 0 N.

a number of hot spots on the surface of Io at short (visible) wavelengths, glowing in the darkness (Fig. 2). The longitudes in darkness of each observation overlapped only between 150 W and 183 W, so the only major hot spot observed in darkness by both instruments during the G1 orbit was South Volund (Davies *et al.* 1997). The South Volund hot spot has since been renamed "Zamama." The hot spots detected by SSI during G1 had to be at temperatures of at least 700 K (McEwen *et al.* 1997). In NIMS data the hot spots were identified by a characteristic thermal ramp, with intensity increasing with increasing wavelength (Lopes-Gautier *et al.* 1997). Single-temperature Planck function fits to NIMS hot spot spectra (covering longer wavelengths than SSI) in the G1INNSPEC01 observation ranged from 384 ± 10 to 606 ± 34 K (Lopes-Gautier *et al.* 1997). From these temperatures alone it was not possible to determine whether the dominating style of volcanism was of silicate or sulfur composition as sulfur may be a liquid at temperatures up to 717 K. However, the shape of the radiative curve at short wavelengths (0.7 to 2 μm) suggested the presence of hotter components on the surface. A two-component fit to the Zamama NIMS data (Davies *et al.* 1997) showed that a small part of the volcano was at a temperature of at least 1100 K (in good agreement with SSI), implying a likely liquidus temperature in excess of 1350 K, well into the range of silicate volcanism. Single-temperature fits to other hot spot spectra (including Prometheus) also resulted in excess fluxes at short wavelengths, suggesting that hotter components were present.

Most of the hot spots identified by Galileo's NIMS and SSI instruments are associated with low-albedo surface features, many identified as dark-floored calderas and flow units (McEwen *et al.* 1997, 1998a, Carr *et al.* 1998, Geissler *et al.* 1999). Descriptions of surface features associated with many of the hot spots observed by Galileo during the Prime mission are given in Lopes-Gautier *et al.* (1997, 1999) and McEwen *et al.* (1998a). Some hot spots are associated with sites of volcanic plumes, most notably Prometheus, which has had a visible plume in every Voyager and Galileo observation having appropriate viewing geometry.

3. OBSERVING WITH NIMS

NIMS is an imaging spectrometer capable of making observations at up to 408 wavelengths over a relatively broad spectral range from 0.7 to 5.2 μm. The operation of the NIMS instrument is described in Carlson *et al.* (1992). The collected data of thermal emission from Io's volcanism are free of absorption features caused by constituents of a thick atmosphere (such as water and carbon dioxide on Earth) and provide the most

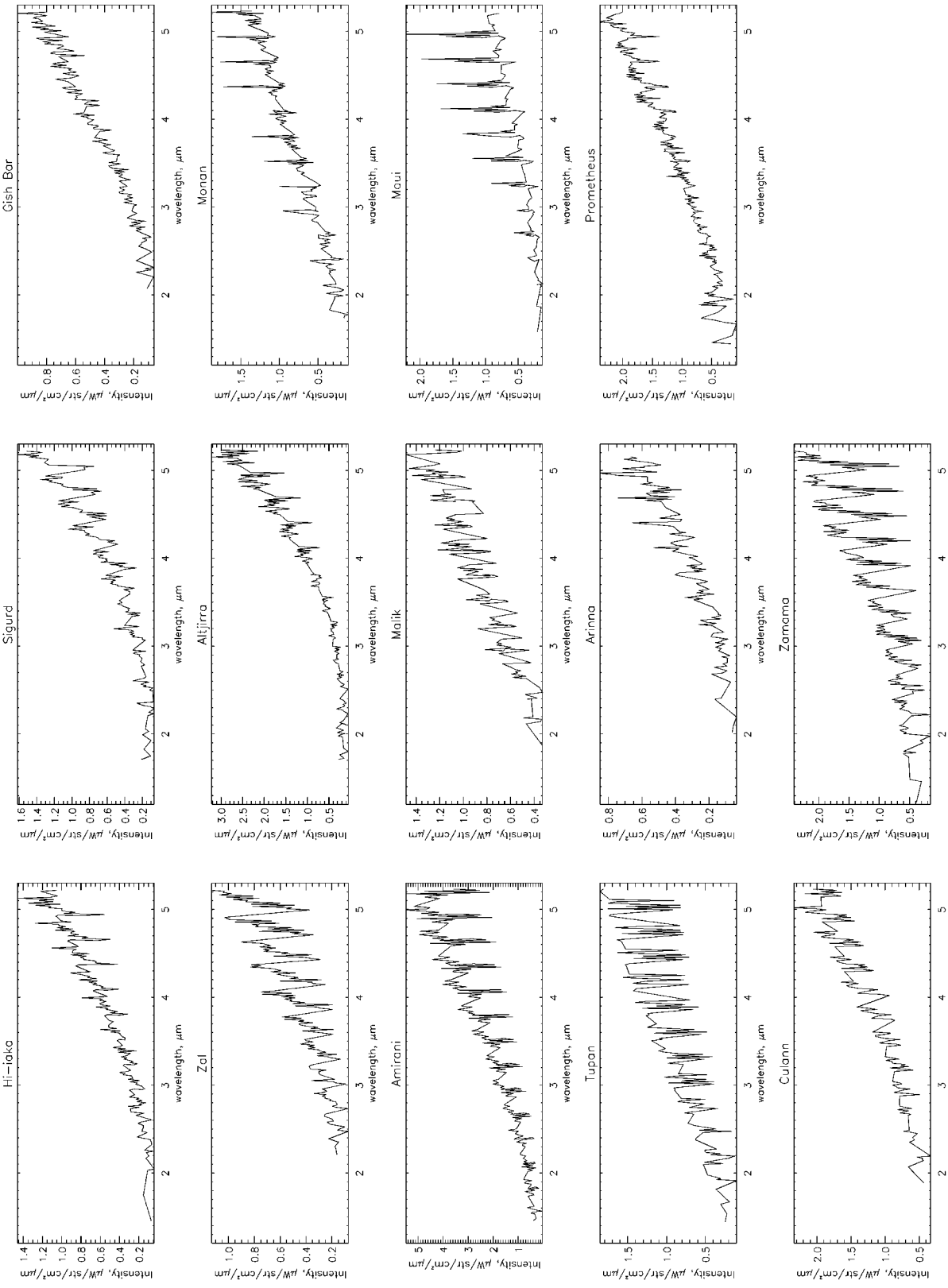

FIG. 3. NIMS spectra for the hot spots analyzed in this paper. Adjacent pixel spectra have been added to take into account the instrument point spread function. Radiation spikes and boom hits have been removed. Dips in the spectra at regular intervals are due to instrument jitter, the result of the instrument field of view moving between acquisition of the spectrum obtained in each grating position.

representative set of data yet obtained of the spectral signature of active volcanism in the 0.7- to 5.2-μm-wavelength range. Due to the distance of Galileo from Io during the G1INNSPEC01 observation (700,750 km) the spatial resolution of the observation is low (350 km/pixel). The volcanically active areas (where material is being emplaced) and most likely all of the inactive areas (stationary, cooling lava) of each hot spot are sub-pixel. By design, most of the G1INNSPEC01 observation is of the nightside of Io so data are uncontaminated by reflected sunlight. In nightside observations NIMS can detect temperatures as low as 180 K, at which temperature the source has to fill the entire NIMS pixel (Smythe *et al.*, 1995). This is a temperature well above the estimated passive background temperature of Io, which never exceeds approximately 130 K at equatorial noon (McEwen *et al.*, 1992). Therefore, all of the emission from a nightside observation detected by NIMS is from thermal anomalies on the surface of Io.

Fourteen major hot spots were observed in darkness in the G1INNSPEC01 observation (see Lopes-Gautier *et al.*, 1997). The criteria for selecting a hot spot as being "major" were given in Lopes-Gautier *et al.* as: (1) a positive slope of the spectrum between 3.5 and 5 μm and (2) an emission at local maximum greater than that of all surrounding pixels. Since the analysis of the G1 data, and in light of subsequent observations (especially in orbit C9), the first condition has had to be modified slightly to take into account other hot spots, most notably at Pele and Pillan, that had spectra with a negative slope between 3.5 and 5 μm due to the peak of thermal emission shifting to shorter wavelengths than that seen in G1 data (Davies *et al.*, 1999).

Table I lists the hot spots analyzed, together with their positions and emission angles as measured from the local planetary normal. For each hot spot, Fig. 3 shows up to 24 sequentially obtained, interleaved spectra, each consisting of up to 17 data points. Each embedded spectrum results from a fixed grating position in the instrument, all 17 points being recorded almost instantaneously. Subsequent spectra of the hot spot are obtained by moving the grating through a series of 24 positions. An individual source takes up only a fraction of a NIMS pixel in the G1INNSPEC01 observation. Small motions of the scan platform during the 24 steps of the observation can result in the image of the hot spot wandering around in the field of view of the detector, with a consequent modulation of the signals in each component 17-point spectrum; this sometimes results in a comb-like appearance to the data. The Prometheus dataset is decomposed into its single-step spectra in Fig. 4. These data, like the data shown in Fig. 3, do not include values obtained when the field of view was intermittently obscured by spacecraft structure. Whether or not this happens is a function of viewing geometry and cone angle (47° for G1INNSPEC01) and is described in Carlson *et al.* (1992). For each hot spot, some grating positions were in near-synchronization with the rotation of the booms and were therefore blocked. This does not affect the remainder of the NIMS spectrum. In analyzing the data, for each hot spot spectrum we take the grating position with the greatest amount of energy under the curve (the "maximum emission" spectrum), as being most representative of the hot spot (covering the largest emitting surface area). There does exist the possibility that the grating position yielding the highest total emission has been blocked by a spacecraft boom: while this would not unduly affect the determination of hot spot age, it would mean that the calculated areas would be underestimated, and this possibility means that areas in this analysis should be considered *minimum* areas.

TABLE I
Hot Spot Positions and Emission Angles

Hot spot	Longitude W	Latitude	Emission angle[a]
Hi'iaka	76	1 S	60.3
Sigurd	100	5 S	37.4
Gish Bar	89	16 N	48.2
Zal	78	43 N	69.4
Altjirra	108	33 S	47.2
Monan	106	19 N	33.1
Amirani	112	27 N	32.6
Malik	127	35 S	41.0
Maui	122	19 N	19.8
Tupan	141	17 S	22.6
Arinna Fluctus	147	36 N	32.9
Prometheus	155	1 S	19.9
Culann	163	18 S	35.5
Zamama	173	21 N	40.3

[a] Sub-spacecraft point = 5 N, 136 W. NIMS resolution at sub-spacecraft point = 350 km/pixel (G1INNSPEC01).

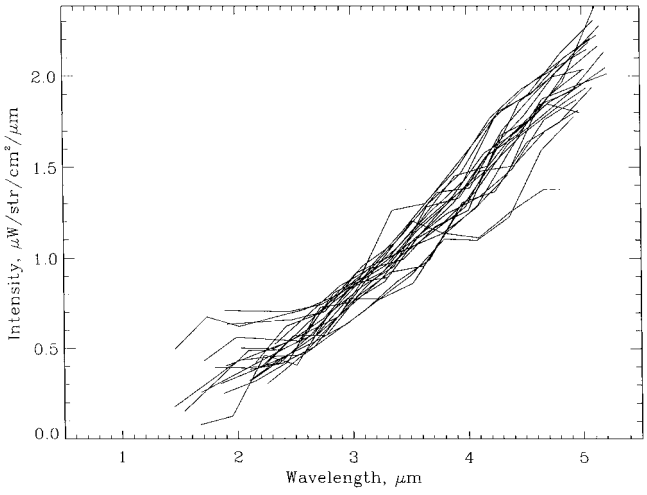

FIG. 4. The NIMS spectrum for Prometheus separated into the spectra obtained in each grating position. A 408 wavelength observation contains 24 17-point spectra, which are free of jitter. Each spectrum is fitted with the cooling model: results are shown in Table III. Three of the grating positions were obscured by spacecraft booms and are not included in this figure.

4. THE SILICATE COOLING MODEL

We use a multiple-temperature silicate cooling model to fit the NIMS G1INNSPEC01 data; a model that describes the

temperature distribution on the surface of a lava body as it is emplaced. The Io Flow Model (IFM), a one-dimensional (depth) silicate cooling model is described in Davies (1996), and was developed to derive the evolving thermal emission from a silicate lava flow or lava lake, and associated vents, on Earth and also on Io. It is partly based on the lava cooling and emplacement model of Head and Wilson (1986). Prior studies of thermal emission from volcanism on Io have been carried out by Sinton (1981), who produced a model for the thermal emission from a sulfur flow, and by Carr (1986), who modeled the thermal signature of active silicate lava flows on Io. Howell (1997) proposed a semiempirical model for active and cooling flows that is akin to the Davies model, generating rates of areal coverage and exposure time (the age of the oldest component). Keszthelyi and McEwen (1997a) also created a magma cooling model to constrain SSI-detected thermal emission. All of these models create a distribution of temperatures on the surface of a lava body as a function of time. Integration over the surface of the lava body yields the thermal emission as a function of wavelength. In the IFM, heat loss from a lava flow takes place by conduction into the ground over which it passes (which does not affect the observed thermal emission) and by radiation from all exposed surfaces. This usually includes radiative heat loss from a high-temperature component in the form of cracks in the crust of the lava, revealing the molten magma beneath (Crisp and Baloga 1990, Flynn and Mouginis-Mark 1992). High-temperature components will be exposed at the vent if fire-fountaining is taking place, along the flow where the crust may be disrupted and through skylights (holes in the roofs of active lava tubes), and at the distal regions of the flow where lava "breakouts" may form. Radiative heat loss from the flow is controlled by the surface temperature and emissivity, and sustained by the ability of the crust (which rapidly forms on newly exposed lava) to conduct heat to the surface. On the anti-jovian hemisphere, for nightside or eclipse Io observations the effective temperature of the environment into which radiation is emitted is 3 K. For parts of Io where Jupiter is in the sky, the planet (with a temperature of ~125 K) can subtend a large enough solid angle to elevate the equivalent background environment temperature to ~43 K. This is insignificant in the modeling at NIMS wavelengths and has negligible effect on the results derived in this paper. The cooling model is attractive as, once the silicate parameters have been selected (including the magma liquidus temperature) and the lava cooling curve calculated for an ionian environment, there are initially only two degrees of freedom: (1) the duration of the eruption needed to produce the observed thermal curve and (2) the total areal extent of the flow, or lava lake surface. Knowing area and eruption duration, the average rate of areal coverage is easily calculated.

An optional refinement to the model (adding another degree of freedom) is the addition of a component at magma liquidus temperature, which represents any exposed areas at liquidus temperatures. A crack fraction (a few percent of total flow surface area) would add flux mostly at short wavelengths, influencing the shape of the lava flow thermal spectrum at these wavelengths (see Flynn and Mouginis-Mark 1992, 1994).

The cooling model calculates the relative areas at different temperatures of the flow surface with time, with the total power output at any given time being determined by

$$F_t = \sum_{i=1}^{i=n_t} A_i \left[T_i^4 (1 - c_\mathrm{f}) + T_\mathrm{s}^4 c_\mathrm{f} \right], \qquad (1)$$

where F_t is the power output (W) at time t, n_t is the number of temperature bins (of size 1 K) at time t (seconds), T_s is the surface temperature (K) at time t, T_i and A_i are bin temperature (K) and area (m^2), respectively, and c_f is a "crack fraction" at magma liquidus temperature. Integrating over all of the areas (for each temperature) yields the emission spectrum for the entire lava body.

4.1. *Model Input Parameters*

In setting up the model, the selection of the magma liquidus temperature parameter has some import: the choice of temperature narrows the range of possible compositions of the magma. What, therefore, is the best model temperature to use to fit to the G1 data? Constraints can be applied. We have seen that a two-temperature fit to Zamama data implies a magma temperature of at least 1350 K. Post-G1 SSI dual-filter observations yielded best-fit single temperatures from 940 to 1675 K for the hottest components of hot spots seen in eclipse (McEwen *et al.* 1998a,b), and fitting the silicate cooling model (using a range of initial magma liquidus temperatures) to a combined NIMS-SSI Pillan dataset from orbit C9 produced an implied magma temperature of *at least* 1870 K (Davies *et al.* 1999), too high a temperature for basalt. Unfortunately, such dual-filter data were not available for the NIMS G1 hot spots.

Model parameters are given in Table II. For the G1 data, the cooling model uses a magma temperature of 1475 K, in the range of temperatures derived from subsequent SSI dual-filter observations. Other thermo-physical parameters are for a dry basalt (see Davies, 1996). Selection of a higher liquidus temperature does not significantly change the eruption ages and areas derived from the NIMS G1 data, because NIMS is not sensitive to

TABLE II
Io Flow Model (IFM) Input Parameters

Model constants		
Io gravity	g	1.8 $\mathrm{m^2\ s^{-1}}$
Environment temperature	T_c	3 K
Model values for silicate (basalt) lava		
Liquidus temperature	T_s	1475 K
Viscosity	η	1500 Pa s
Thermal conductivity	k	0.6 $\mathrm{W\ m^{-1}\ K^{-1}}$
Liquid density	ρ	2600 $\mathrm{kg\ m^{-3}}$
Yield strength of liquid	τ	100 Pa
Latent heat of fusion	Q	4×10^5 $\mathrm{J\ kg^{-1}}$
Specific heat capacity	c	1500 $\mathrm{J\ kg^{-1}\ K^{-1}}$
Emissivity	ε	1

very high temperature components if they have very small areas (which results in low signal-to-noise ratios for detectors 1 and 2, at the shortest NIMS wavelengths). Increasing the instrument gain to better see these components might have led to saturation at longer wavelengths. The cooling model predicts that the higher the surface temperature, the smaller the area at this temperature as the cooling rate is a function of (temperature)^4; for example, of a flow 10 days into an eruption, the area between 1900 and 1400 K is only 0.001% of the total area. This effect is exacerbated by the low spatial resolution of G1INNSPEC01: the smallest, hottest areas may not be seen. In the absence of short-wavelength constraints on thermal emission (such as SSI dual-filter observations), we cannot say anything more specific regarding magma liquidus temperature from the G1 NIMS data beyond that it is characteristic of silicate composition.

4.2. Thermal Emission and Eruption Style

What does the shape of the thermal emission curve tell us about eruption style? Different eruption styles should exhibit different thermal emission curves. In its simplest application, the cooling model assumes that, as an eruption continues, the surface of the erupted lava body steadily increases in areal extent. At the onset of the eruption, the area of the lava is small and at high temperatures, close to the magma liquidus temperature, and so maximum thermal emission from the flow is at a short wavelength. As time passes the distal areas of the flow cool, and the wavelength of maximum emission of the integrated surface area increases. The shape of the thermal spectrum therefore contains temporal information about the eruption. Figure 5 shows how the model emission spectrum for an active lava flow changes with time, and Fig. 6 shows the change in wavelength of maximum emission with time. Davies (1996) showed how this thermal evolution could be applied to an overturning lava lake. With time, the thermal trends of flows and lakes should diverge: flows spread, creating large cool areas, while active lakes overturn regularly, destroying any cool surface crust. The cooling model can also reproduce the thermal emission from fire fountains. An active fire-fountain event was observed on Io at Tvashtar by Galileo SSI during the I25 encounter in November 1999 (McEwen *et al.*, 2000), and fire fountains have most likely been observed on Io in the past (Davies 1996, Stansberry *et al.* 1997) with timescales similar to those of terrestrial events (hours to days). Fire fountains have a preponderance of thermal emission at very short wavelengths, and the thermal signature of such an event should be very different from that expected from (for example) the laminar emplacement of a lava flow.

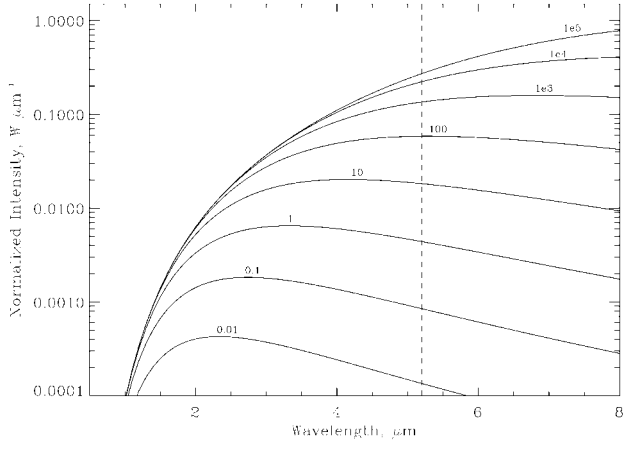

FIG. 5. The normalized spectral signature of an active flow with time. As the distal ends of the flow cool, the temperature distribution on the surface of the flow changes: as it does so, so does the resulting emission spectrum. The best-fitting curve for each NIMS spectrum is found using a least-squares algorithm. The figure above each curve shows the eruption duration in hours. The NIMS wavelength range lies between the vertical dashed lines.

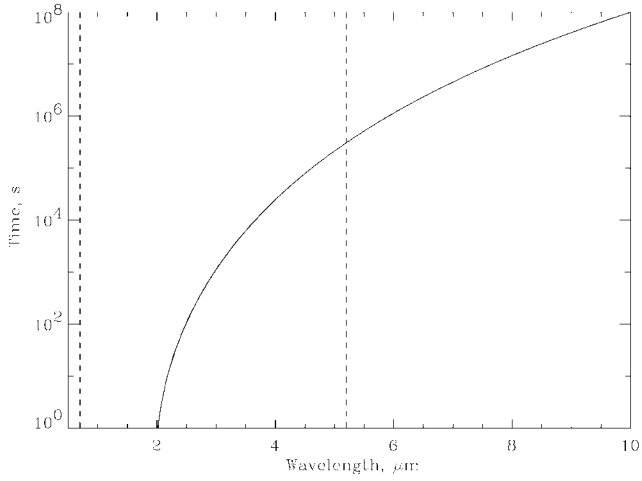

FIG. 6. The change in wavelength of maximum emission with time from the silicate cooling model. This figure is a representation of the changing shape of the emission curve from an evolving lava flow. With time, as cooler components form, the wavelength of maximum emission of the integrated power output increases. The NIMS wavelength range lies between the vertical dashed lines.

5. APPLICATION OF THE COOLING MODEL TO NIMS DATA

The NIMS data are fitted with the model output as follows. The synthesized emission spectra produced by the model are iteratively fitted to the NIMS data to find the "best-fit" model curve for each grating position spectrum, yielding an eruption duration. For each hot spot, the "maximum emission" grating position is found (see section 3). The average duration and standard deviation are calculated, and these values are used to refit the "maximum emission" spectrum, to produce (1) the area of the hot spot, using the average duration, and (2) the uncertainty in the hot spot area, using the standard deviation of the durations.

6. RESULTS

6.1. Eruption Duration and Area

The model fits to the "maximum emission" grating position spectrum for each hot spot are shown in Fig. 7. Taking

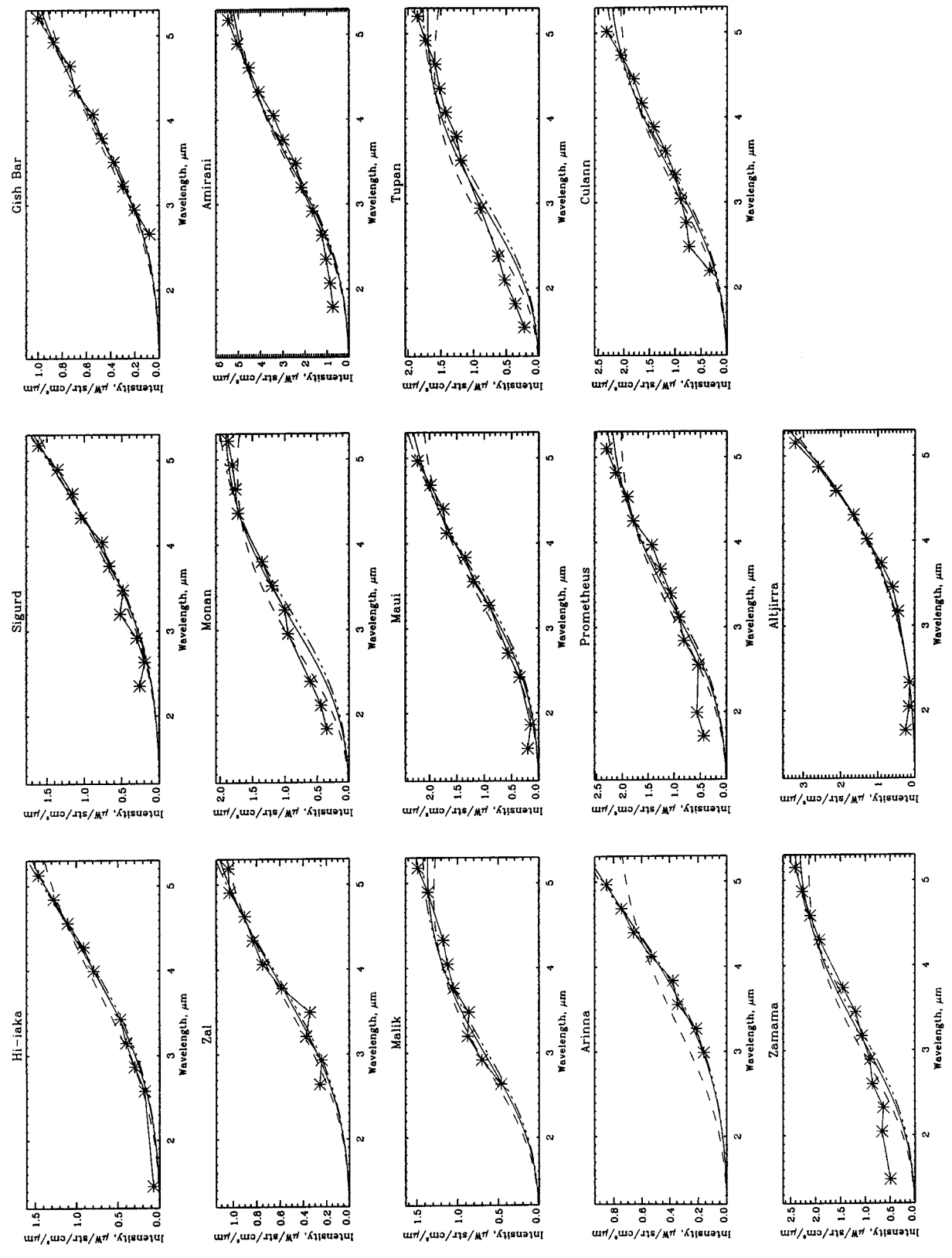

FIG. 7. Fits to the 14 G1 hot spot spectra using the Io Flow Model. The spectra shown here are the "maximum emission" spectra (stars), most representative of the hot spot emission. Each spectrum is fitted with the average eruption duration for that hot spot (solid line). The uncertainties of the fit are shown as the dotted and dashed lines: the areas and durations are listed in Table IV. With Altjirra the model reaches the NIMS lower temperature detection threshold. The fits shown may model temperatures down to 180 K (solid line), and the shortest eruption duration from fitting all of the grating position spectra (dashed line) is taken as the minimum possible age, also yielding the smallest calculated area.

TABLE III
Grating Position, Eruption Duration, and Related Model Index for Prometheus

Grating position	Model eruption duration ($\times 10^5$ s)	Lowest surface temperature (K)
1	9.40	406
2	2.48	473
3	6.58	423
4	3.11	461
5	5.71	430
6	3.55	454
7	8.45	411
8	5.71	430
9	9.40	406
10	6.58	423
11	12.2	394
12	8.45	411
13	15.2	384
14	9.40	406
15	21.9	368
16	3.42	465
17	10.9	399
18	10.9	399
19	No data: obscured by boom	
20	No data: obscured by boom	
21	10.9	399
22	7.61	416
23	10.9	399
24	No data: obscured by boom	

Note. Average duration, 8.71×10^5 s (10 days); standard deviation, 4.48×10^5 s (5 days).

Prometheus as an example, Table III shows the eruption durations calculated for each grating position. Prometheus has an eruption duration of 10 days (±5 days) with the coolest part of the flow having cooled down to about 400 K. The area of the active region is 30 km^2. It is interesting to note that the derived area for Prometheus is only part of an extensive area of lava flows, including the vents of the Prometheus volcanic plume (McEwen *et al.* 1998b) that have been erupting since the Voyager encounters in 1979 and which are still being emplaced. During G1, NIMS apparently observed the most recent of a continuous series of eruptive episodes. The lack of temperature components below 400 K might be indicative of emplacement mechanism, with cooler (and therefore older) components being buried by younger material. This is a process common on the floors of calderas, and in pahoehoe flow fields. Alternatively, the older flows may be relatively thin, quickly solidifying, and cooling to below NIMS detection levels.

The hot spot with the widest range of eruption ages is Arinna Fluctus, with an average eruption duration of 250 days and a standard deviation of 237 days. It might be that there is more than one volcanic center in the Arinna Fluctus pixels: if separated spatially by a large enough distance, this could lead to changes in the shape of individual grating spectra relative to one another when adjacent pixels are added to account for the instrument point spread function, finally producing a larger spread of derived eruption times. Altjirra seems to fall into a different class than the other hot spots and is discussed in more detail in section 7.3.

Table IV shows the eruption ages, which range from 3 days (Tupan) to 18 years (Altjirra). Hot spot areas corrected for emission angle are also shown in Table IV. With the exception of Altjirra, hot spot areas range from 12 km^2 (Tupan) to 280 km^2 (Sigurd). The Altjirra hot spot has an area of nearly 20,000 km^2 and a temperature range apparently down to 180 K, the detection limit of NIMS. Hot spot areas and ages are shown in Fig. 8.

From Fig. 7, Amirani, Prometheus, Monan, Tupan, and Zamama have emission at wavelengths less than 3 μm that is in excess of model predictions. It is noted that model fits to these spectra are slightly improved by the addition of a small area (typically less than 0.1% of the whole active area) at magma liquidus temperatures, the "crack fraction" already discussed. However, the improvement in the fit to the data of including a crack fraction is not significant (using the f test, applied to the Zamama data). This is partially due to the fact that the silicate cooling model already includes components at high temperatures, accounting for some of the crack fraction flux. Accordingly, the fits to the G1 data are presented without the additional crack fraction parameter.

6.2. Areal Coverage Rates and Thermal Output

Using derived eruption duration and area, the average rate of areal coverage (dA/dt) for individual eruptions can be calculated; these are shown in Table V. Coverage rates range from

TABLE IV
Eruption Duration and Area for Main G1 Hot Spots

Hot spot	Eruption age (days)	Area (km^2)[a]
Hi'iaka	139 ± 103	248 ± 149
Sigurd	268 ± 135	280 ± 131
Gish Bar	64 ± 32	65 ± 27
Zal	44 ± 22	108 ± 43
Altjirra[b]	28 years, −23 years[b], + ?	18,600,–15,400, + ?
Monan	6 ± 4	22 ± 10
Amirani	15 ± 5	102 ± 24
Malik	4 ± 1	13 ± 4
Maui	21 ± 12	49 ± 21
Tupan	3 ± 2	12 ± 5
Arinna Fluctus	250 ± 238	148 ± 131
Prometheus	10 ± 5	30 ± 11
Culann	12 ± 9	39 ± 14
Zamama	7 ± 4	32 ± 12

[a] Areas have been corrected for emission angle (see Table 1) such that corrected area = derived area/cos (emission angle).

[b] With the Altjirra data the model runs up against the low-temperature detection limit of the NIMS instrument. The Altjirra area is derived for the temperature range down to 180 K. The lower limit is determined from the youngest age derived from fitting the individual grating position spectra. It is not possible to determine whether there are cooler components (of greater age) from NIMS data alone.

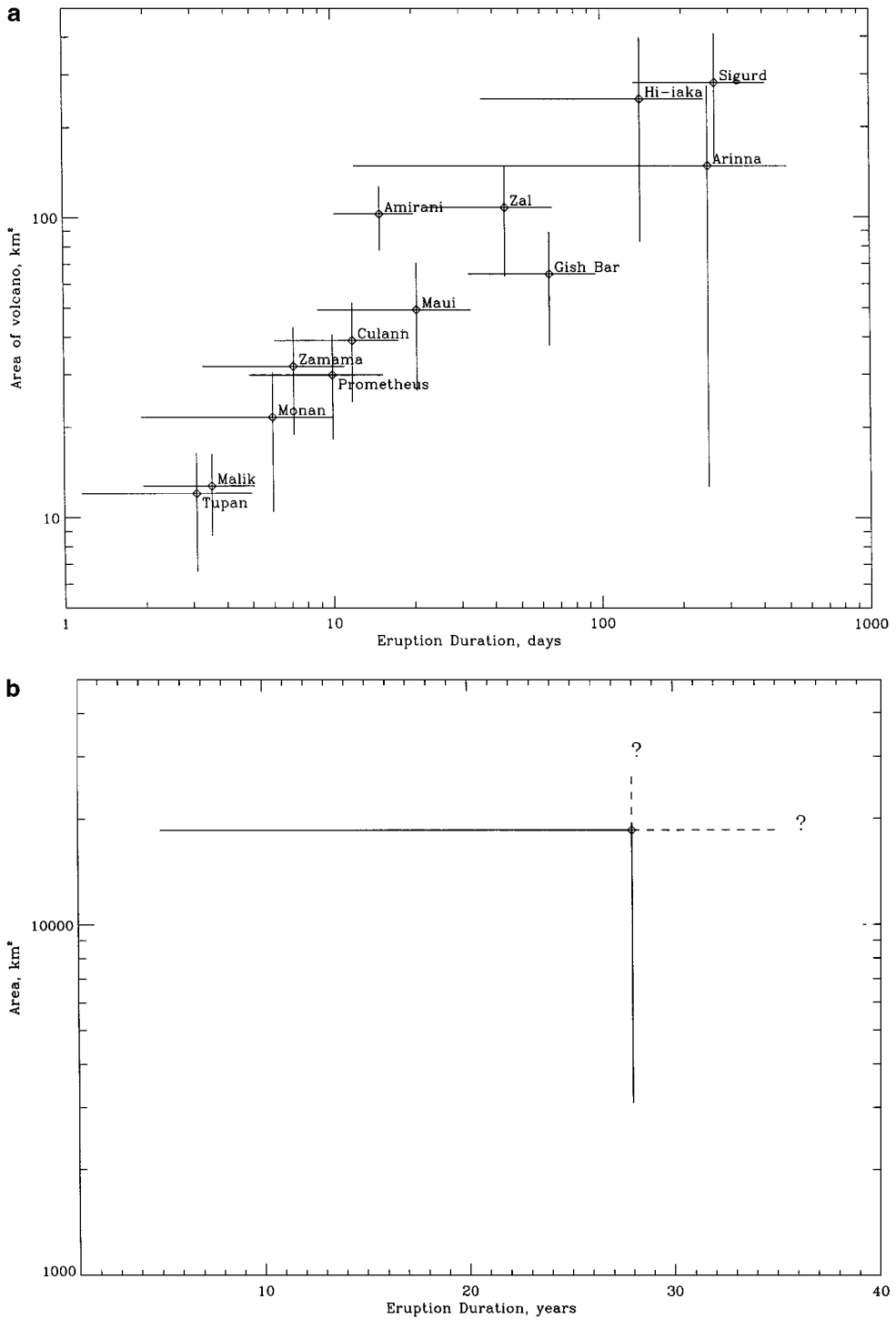

FIG. 8. (a) Eruption durations and sizes for thirteen hot spots analyzed from the G1INNSPEC01 observation dataset, excluding Altjirra. Durations and sizes run from 3 days and 12 km^2 (Tupan) to 268 days and 280 km^2 (Sigurd). (b) The fit to the Altjirra data. The minimum age for Altjirra is 5 years with an area of 3100 km^2. The duration determined using a minimum temperature of 180 K (the NIMS low-T detection limit) is 28 years, with an area of 18,000 km^2.

7 m^2 s^{-1} (Arinna Fluctus) to 79 m^2 s^{-1} (Amirani), and the total area covered by these eruptions per second is 457 m^2. The thermal outputs from the hot spots are also shown in Table V and range from 5.76×10^{10} W at Tupan to 2.10×10^{12} W at Altjirra. The total energy from these 14 hot spot is 3.56×10^{12} W, from 37% of Io's surface. Assuming a random longitudinal distribution of hot spots this normalizes to approximately 10^{13} W globally, or approximately 10% of Io's total radiometric thermal

TABLE V
Areal Coverage Rates, Mass Eruption Rates, and Power Output

Hot Spot	Implied dA/dt ($m^2\ s^{-1}$)	Upper dA/dt limit ($m^2\ s^{-1}$)	Lower dA/dt limit ($m^2\ s^{-1}$)	Mass eruption rates: 1-m-thick flow ($m^3\ s^{-1}$)	Thermal output from hot spot ($\times 10^{10}$ W)
Hi'iaka	20	26	19	20	17.43
Sigurd	12	13	11	12	16.20
Gish Bar	12	13	11	12	6.82
Zal	28	33	26	28	15.22
Altjirra	21	22	≤21	21	210.0
Monan	41	63	35	41	7.34
Amirani	79	88	73	79	24.28
Malik	41	51	37	41	5.96
Maui	27	35	25	27	9.69
Tupan	45	66	38	45	5.76
Arinna Fluctus	7	12	6	7	9.33
Prometheus	35	43	32	35	8.62
Culann	38	46	34	38	9.25
Zamama	51	67	45	51	10.59
Total	457	578	≤418	457	356

output of 10^{14} W (Veeder *et al.*, 1994). The global thermal emission, as derived from the G1 volcanoes, compares favorably with the Veeder *et al.* estimate of 1.13×10^{13} W for the 1983–1993 average thermal emission from sources at temperatures greater than 200 K. This indicates that the hot spot activity observed on the leading/anti-jove hemisphere observed in G1INNSPEC01 is probably typical, and a good indication of the background (non-outburst) level of volcanic activity.

6.3. Estimated Flow Thickness and Global Effusion Rate

A global thermal contribution from hot spots of 10^{13} W yields a flux of 3×10^{20} J per year. This figure places a constraint on global effusion rates, and on average lava flow thickness, by considering the heat content of the erupted material, assuming (1) a steady rate of production of lava at the surface and (2) that the number and distribution of large hot spots remains more or less constant (and this has been borne out by analysis of subsequent observations by NIMS and SSI: see Lopes-Gautier *et al.* 1999). Lava contains both latent and specific heats (see Table II), which are liberated as the lava solidifies and cools to ionian ambient temperatures (90–130 K). Some of this energy will be conducted down into the ground beneath the lava flow: most, however, will be conducted through the flow's upper crust and radiated away over time. The volume of basalt containing a total latent heat and heat lost through cooling of 3×10^{20} J is approximately 43 km^3. This is the volume of material that has to be erupted every year to produce the observed G1 hot spot emission. In terms of volumes erupted per second, the mass fluxes are 1363 $m^3\ s^{-1}$ globally, or 504 $m^3\ s^{-1}$ for the hot spots in G1INNSPEC01. If the total rate of areal coverage for these hot spots is 457 $m^2\ s^{-1}$ then the average thickness of the lava flows is slightly more than 1 m. Mass eruption rates, calculated using this thickness, are shown in Table V: the rates range from 7 $m^3\ s^{-1}$ (Arinna Fluctus) to 79 $m^3\ s^{-1}$ (Amirani).

7. DISCUSSIONS

7.1 Model Fits and Emplacement Mechanism

How realistic are the model fits to the data? Good fits to the data (see Fig. 7) can be obtained with the cooling model even though the model assumes a single flow lobe, which is an oversimplification of the emplacement mechanism of silicate magma. For example, Hawaiian eruptions typically produce an overlapping series of small pahoehoe and a–a flows making up a flow field. Only occasionally does the emplacement of a large, single-lobe flow dominate extrusive activity. However, the goodness of model fit to the G1 NIMS data indicates that, whatever the complexities of lava flow emplacement, the resulting distribution of temperatures over the whole volcanic edifice generally follows a distribution of temperatures predicted by the cooling model. Howell (1997), who also uses a single-lobe model, addresses this apparent oversimplicity succinctly, noting that, first, the thermal emission process is well understood and *is* inherently simple, and second, that the emplacement mechanism, while multi-faceted, ultimately consists of component processes that can be characterized statistically in terms of rate of production of surface area and timescale, the processes averaging out to produce the final areal rate and flow age output by the model. It should be noted that the model predicts that the thermal signature from a single-lobe flow is the same as that from (for example) two separate flows of half the areal coverage rate, as long as they have the same start time and lie within the same NIMS pixel. Indeed, high-resolution imaging of the surface of Io (SSI at 9 m/pixel and NIMS at 500 m/pixel) took place during orbit I24 in October 1999, and again during I25 (November 1999) and I27 (February 2000), and some hot spots were found to be made up of two or three smaller active components (for example, Prometheus and Maui/Amirani; see Lopes-Gautier *et al.*, 2000). It is most probable that the areal coverage rates determined from the G1

data are apportioned between multiple flow lobes for some hot spots, including Prometheus, Amirani, and Maui.

7.2 Mass Eruption Rates and Resurfacing of Io

Even assuming a 10-m average flow thickness, the implied mass eruption rate for each hot spot is relatively small when compared with the largest observed terrestrial mass eruption rates. Laki, for example, had a maximum mass eruption rate of 8700 $m^3\ s^{-1}$ (Thordarson and Self 1993). The G1 mass fluxes are more comparable to relatively low-viscosity basalt eruptions: Kilauea Iki had a maximum mass eruption rate of 100 $m^3\ s^{-1}$; Kilauea has an overall mass eruption rate of 2 to 600 $m^3\ s^{-1}$ (Malin 1980); and Mauna Loa has overall mass eruption rates from 10 to 1000 $m^3\ s^{-1}$ (Malin 1980). The NIMS-derived mass eruption rates are especially modest when compared with implied mass eruption rates for the large Io thermal outbursts, such as Loki, 1990 ($dA/dt = 10^5\ m^2\ s^{-1}$, mass eruption rate $= 1.7 \times 10^5\ m^3\ s^{-1}$ (Blaney *et al.*, 1995); $dA/dt = 8.7 \times 10^4\ m^2\ s^{-1}$, mass eruption rate $= 7.7 \times 10^5\ m^3\ s^{-1}$ (Davies 1996)).

It must be remembered that the global eruption figure is derived from the "large" G1 hot spots, where there is an appreciable increase in 4.8-μm emission above that from nearby "background" pixels. In high-resolution NIMS images of Io, small hot spots have been discovered that that would not have been identified as "major" in G1INNSPEC01. This means that the mass eruption rate above is derived from what is in fact a selection of hot spots and is therefore a minimum value for silicate emplacement.

Finally, given a yearly volume of production of 43 km^3, the global resurfacing rate from large hot spots (not including outburst events) is 0.1 cm/year. This happens to be the resurfacing rate of Io as determined by Johnson and Soderblom (1982), based on crater burial rates and assuming a Lunar impact flux. Shoemaker (1994) estimated that the impact flux in the jovian system was approximately 10 times the lunar rate, and so, applying the Johnson and Soderblom (1982) model, the Io resurfacing rate becomes 1 cm/year. Blaney *et al.* (1995) estimated a resurfacing rate of $\sim$1.3 cm/year based on Io's heat flow, and Zahnle *et al.* (1998), in a recalculation of cratering rates in the jovian system, estimated a resurfacing rate for Io of at least 0.4 cm/year. The discrepancy between the rate of lava production and resurfacing rate has to be made up by resurfacing from other sources, such as plumes, rare "outburst" events, and eruptions of lower melt-temperature materials, such as sulfur, to which NIMS is less sensitive.

7.3 Hot Spot Surface Temperature Ranges

Model fits yield a range of areas and temperatures for each volcano. For most of the hot spots the resulting temperature range implied by model fits is well above the detection threshold of NIMS. For a long-lived hot spot like Prometheus the implication is that much of the flow surface is at temperatures below NIMS detection levels, or are at low enough temperatures that their contribution to the NIMS spectrum is swamped by emission from the higher-temperature material.

Altjirra is the only one of the G1 hot spots where the modeled surface temperature range is down to the detection limit of NIMS (180 K), the fit implying that most of the area is at temperatures between 200 and 180 K. This highlights a problem arising from fitting the model to NIMS data: eventually, the 0.7- to 5.2-μm model spectrum stops changing as the effective addition of cooler components would have no effect on what NIMS observes (see Fig. 5). In the case of Altjirra, therefore, the cooling model can provide only a lower limit to the age of the flows, and accordingly, a lower limit only to the area of the flows. There may be larger and cooler components present, but NIMS cannot be expected to see them. Although the location of Altjirra is not associated with any observed groundbased thermal outburst, SSI did image new post-Voyager dark, flow-like deposits here (McEwen *et al.* 1998a). This would limit the flow ages to about 17 years, the period between Voyager and Galileo G1. The youngest age obtained from fitting the individual grating position spectra is about 5 years, still greater than the ages determined at all the other hot spots. Assuming that there was no hot spot activity during the Voyager encounters, that is, that the eruption was entirely post-Voyager, by setting the maximum possible age of Altjirra to 17 years the best fit to the data yields an area of approximately 11,400 km^2, an average rate of emplacement of 21 m^2/s, and a total energy output of 1.64×10^{12} W, about 20% less than the energy output expected with the model running to the low-temperature limit.

SSI did not see a hot spot at Altjirra, nor would it have: the total area at temperatures in excess of 700 K (to which SSI is sensitive) is less than 0.5 km^2. Altjirra might be the site of an old eruption, where deposits and lava flows have been covered or faded to background colors and albedos, or may be a large geothermal area, at temperatures higher than the rest of the nonvolcanic surface. However, the Altjirra hot spot does have a small active component, which contributes the short-wavelength thermal emission observed by NIMS. Altjirra appears to be a more complex eruption than the other large hot spots in G1INNSPEC01. It is characteristic of a small, relatively new eruption at an extensive old (and therefore cool) eruption site, or "warm" area.

7.4 Eruption Style and Thermal Signature, Revisited

The model fits to the G1 data imply that the eruption emplacement style is predominantly laminar, consisting of one or more flow lobes with relatively stable surface crusts. A pahoehoe field, consisting of relatively smaller multiple flow lobes (but also emplaced in a laminar regime) would evolve a similar temperature distribution: assuming that the entire field is sub-pixel, the thermal emission spectrum would be dominated at longer NIMS wavelengths by a large area of older material, and the shorter wavelength components would be dominated by emission from the active lobes of the flow field.

It should be possible to identify different emplacement styles from the shape of the thermal emission spectrum. If magmas are

(for example) of a high-melt-temperature, low-viscosity composition, a large-volume eruption might result in flows that are turbulently emplaced, (an emplacement mechanism proposed for some komatiite flows on Earth in Archean times). This would initially prevent a crust forming on the surface of the flow, and as a result, more of the interior of the flow at high temperature will be exposed. A surface temperature of 1475 K emits its maximum energy at 2 μm. The G1 hot spots mostly exhibit peak emission at wavelengths longer than 4.8 μm (where a body at 600 K emits maximum energy). More than a few percent of the flow surface area at magma liquidus temperatures would lead to the preponderance of thermal emission moving to shorter wavelengths than that observed for a less energetic, more laminar emplacement mechanism which leads to the formation of a stable surface crust. The shapes of the G1 hot spot spectra do not exhibit the thermal emission at short wavelengths (less than 2 μm) that would be expected from a large, turbulently emplaced flow. Post-G1 observations of Pele and Pillan (see Davies *et al.* 1999) show extensive emission at short wavelengths and are not well-fitted with a "single-lobe" model. These data are indicative of a more complex and different style of emplacement from that implied by G1INNSPEC01 analysis.

7.5 Emission at Shorter and Longer Wavelengths

These results from the NIMS G1 data are biased toward the high-temperature components of volcanic activity, due to the wavelength range of the NIMS instrument. Model fits to the NIMS data can be further constrained by considering other data sets. Short wavelength data from the SSI instrument have been used with NIMS data in a mutually constraining analysis of C9 data of Pele and Pillan (Davies *et al.* 1999) and longer wavelength data from the Photo-Polarimeter Radiometer on Galileo and from groundbased observations can be used to better constrain and model thermal emission from Io's hot spots. To facilitate this effort, Table VI shows the measured 3.5-, 4.8-, and predicted 8.7-, 12-, and 20-μm fluxes from the best model fits to the G1INNSPEC01 hot spot data.

TABLE VI
Cooling Model Fluxes in GW/str/μm

Volcano	3.5 μm	4.8 μm	8.7 μm	12 μm	20 μm
Hi'iaka	1.28	3.14	5.20	3.78	1.28
Sigurd	0.78	2.07	4.14	3.27	1.21
Gish Bar	0.69	1.53	2.02	1.34	0.41
Zal	1.62	3.41	4.04	2.57	0.76
Monan	1.76	2.70	1.89	0.99	0.24
Amirani	3.94	7.01	6.21	3.54	0.93
Malik	1.55	2.19	1.36	0.68	0.16
Maui	1.45	2.71	2.61	1.53	0.42
Tupan	1.62	2.24	1.35	0.67	0.15
Arinna F.	0.44	1.15	2.26	1.78	0.65
Prometheus	1.61	2.69	2.14	1.17	0.30
Culann	1.64	2.99	2.76	1.59	0.43
Zamama	2.25	3.56	2.61	1.39	0.34
Altjirra[a]	1.39	4.41	22.39	30.87	22.04
Altjirra[b]	1.46	4.40	14.79	15.25	7.59

[a] For minimum surface temperature of 180 K.

[b] For minimum surface temperature of 221 K, corresponding to an age of 5 years. This is the youngest eruption duration obtained from fits to the individual grating position spectra.

8. CONCLUSIONS

The G1INNSPEC01 observation is an excellent example of the normal, background level of activity on Io for the leading/anti-jove hemisphere. The thermal emission spectra of the hot spots observed by NIMS during orbit G1 are consistent with silicate lava flow emplacement, in a relatively quiescent emplacement regime without turbulent flows forming to a significant extent. The calculated eruption durations for these hot spots range from a few days to decades, these durations referring to those parts of the volcanic edifices contributing to thermal emission in the 0.7- to 5.2-μm range. Most of the volcanoes appear to have maximum "lava exposure" times of less than a few weeks. The exception is Altjirra, the hot spot with the greatest age of activity and the greatest area. Altjirra appears to be a hybrid: there is little evidence of flows of the size expected from the cooling model fits, although they might have been covered over the years. Altjirra might be one of the class of large, cool, persistent thermal anomalies below 200 K suggested by Veeder *et al.* (1994), but does contain a small active region.

The major hot spots on the leading/anti-jovian hemisphere contribute about 5% of Io's thermal budget, normalized to 10% for all of Io. Mass eruption rates obtained are comparable to terrestrial (basalt) eruptions, and are considerably less than those found by investigators calculating "outburst" mass eruption rates (10^5–10^6 m^3 s^{-1}). Applying the resurfacing rate for the area covered by the G1INNSPEC01 observation to all of Io, and assuming an average flow thickness of 1 m, a global resurfacing rate of 0.1 cm/year is derived. This is about 10% of that derived by Shoemaker (1994). The discrepancy has to be made up from other resurfacing mechanisms.

ACKNOWLEDGMENTS

Thanks are due to the members of the Galileo NIMS Team especially Frank Lender, Lucas Kamp, and Bob Mehlman, and Galileo mission and the Io Working Group, especially Diana Blaney, Bob Howell, Jay Goguen, Torrence Johnson, Laszlo Keszthelyi, Dennis Matson, Alfred McEwen, John Spencer, and John Stansberry. A.G.D. wishes thanks to Jim Shirley for his thoughtful review of the manuscript. The article benefited greatly from reviews by John Stansberry and an anonymous reviewer. This work was carried out under NASA contract at the Jet Propulsion Laboratory—California Institute of Technology, Pasadena, California.

REFERENCES

Belton, M. J. S., and 22 colleagues 1992. The Galileo solid-state imaging experiment. *Space Sci. Rev.* **60**, 413–455.

Belton, M. J. S., and 33 colleagues 1996. Galileo's first images on Jupiter and the Galilean satellites. *Science* **274**, 337–385.

Blaney, D. L., T. V. Johnson, D. L. Matson, and G. J. Veeder 1995. Volcanic eruptions on Io: Heat flow, resurfacing and lava composition. *Icarus* **113**, 220–225.

Carlson, R. W., P. R. Weissman, W. D. Smythe, and J. C. Mahoney 1992. Near Infrared Mapping Spectrometer experiment on Galileo. *Space Sci. Rev.* **60**, 457–502.

Carr, M. H. 1986. Silicate volcanism on Io. *J. Geophys. Res.* **91**, 3521–3532.

Carr, M. H., A. S. McEwen, K. A. Howard, F. C. Chuang, P. Thomas, P. Schuster, J. Oberst, G. Neukum, G. Schubert, and the Galileo SSI Team 1998. Mountains and calderas on Io: Possible implications for lithospheric structure and magma generation. *Icarus* **135**, 146–165.

Crisp, J., and S. Baloga 1990. A model for lava flows with two thermal components. *J. Geophys. Res.* **95**, 1255–1270.

Davies, A. G. 1996. Io's volcanism: Thermo-physical models of silicate lava compared with observations of thermal emission. *Icarus* **124**, 45–61.

Davies, A. G., A. S. McEwen, R. M. C. Lopes-Gautier, L. Keszthelyi, R. W. Carlson, and W. Smythe 1997. Temperature and area constraints of the South Volund volcano on Io from the NIMS and SSI instruments during the Galileo Gl orbit. *Geophys. Res. Lett.* **24**, 2447–2450.

Davies, A. G., L. P. Keszthelyi, R. M. C. Lopes-Gautier, A. S. McEwen, W. D. Smythe, L. Soderblom, and R. W. Carlson 1999. Thermal signature, eruption style and eruption evolution at Pele and Pillan Patera on Io. *Proc. Lunar. Planet. Sci. Conf. 30th*. [abstract on CD-ROM]

Flynn, L. P., and P. J. Mouginis-Mark 1992. Cooling rate of an active Hawaiian lava flow from nighttime spectroradiometer measurements. *J. Geophys. Res.* **19**, 1783–1786.

Flynn, L. P., and P. J. Mouginis-Mark 1994. Temperature of an active lava channel from spectral measurements, Kilauea Volcano, Hawaii. *Bull. Volcanol.* **56**, 297–301.

Geissler, P. E., A. S. McEwen, L. P. Keszthelyi, R. Lopes-Gautier, J. Granahan, and D. P. Simonelli 1999. Global color variations on Io. *Icarus* **140**, 265–282.

Goguen, J. D., P. D. Nicholson, T. L. Hayward, J. E. Van Cleve, G. J. Veeder, D. L. Blaney, D. L. Matson, and T. V. Johnson 1998. A comparison of two eruptions on Io. *Proc. Lunar Planet. Sci. Conf. 29th.* [abstract]

Head, J. W., and L. Wilson 1986. Volcanic processes and landforms on Venus: Theory, predictions and observations. *J. Geophys. Res.* **91**, 9407–9466.

Howell, R. R. 1997. Thermal emission from lava flows on Io. *Icarus* **127**, 394–407.

Howell, R. R., J. R. Spencer, and J. A. Stansberry 1998. IR occultation observations of volcanic hot spots on Io. *Proc. Lunar Planet. Sci. Conf. 29th.* [abstract]

Johnson, T. V., and L. A. Soderblom 1982. Volcanic eruptions on Io: Implications for surface evolution and mass loss. In *Satellites of Jupiter* (D. Morrison, Ed.), pp. 634–646. Univ. Arizona Press, Tucson.

Johnson, T. V., G. J. Veeder, D. L. Matson, R. H. Brown, R. M. Nelson, and D. Morrison 1988. Io: Evidence for silicate volcanism in 1986. *Science* **242**, 1280–1283.

Keszthelyi, L. P., and A. S. McEwen 1997a. Thermal models for basaltic volcanism on Io. *Geophys. Res. Lett.* **24**, 2463–2466.

Keszthelyi, L. P., and A. S. McEwen 1997b. Magmatic differentiation of Io. *Icarus* **130**, 437–488.

Lopes-Gautier, R., S. Doute, W. D. Smythe, L. W. Kamp, R. W. Carlson, A. G. Davies, F. E. Leader, A. S. McEwen, P. E. Geissler, S. W. Keiffer, L. P. Keszthelyi, E. Barbinis, R. Mehlman, M. Segura, J. Shirley, and L. A. Soderblom 2000. A close-up look at Io from Galileo's Near-Infrared Mapping Spectrometer. *Science* **288**, 1201–1204.

Lopes-Gautier, R., A. S. McEwen, W. D. Smythe, P. E. Geissler, L. Kamp, A. G. Davies, J. R. Spencer, L. Keszthelyi, R. Carlson, F. E. Leader, R. Mehlman, L. Soderblom, and the Galileo NIMS and SSI Teams 1999. Active volcanism on Io: Global distribution and variations in activity. *Icarus* **140**, 243–264.

Lopes-Gautier, R. M. C., A. G. Davies, R. Carlson, W. Smythe, L. Kamp, L. Soderblom, F. E. Leader, R. Mehlman, and the Galileo NIMS Team 1997. Hot spots on Io: Initial results from Galileo's Near Infrared Mapping Spectrometer. *Geophys. Res. Lett.* **24**, 2439–2442.

Malin, M. C. 1980. The lengths of Hawaiian lava flows. *Geology* **8**, 306–308.

Matson, D. L., D. L. Blaney, T. V. Johnson, G. J. Veeder, and A. G. Davies 1998. Io and the early Earth. *Proc. Lunar Planet. Sci. Conf. 29th*. [abstract on CD-ROM]

McEwen, A. S., and 24 colleagues 2000. Galileo at Io: Results from high-resolution imaging. *Science* **288**, 1193–1198.

McEwen, A. S., N. R. Isbell, and J. C. Pearl 1992. Io thermophysics: New models with Voyager 1 thermal IR spectra. *Proc. Lunar Planet. Sci. Conf. 23rd*, 881.

McEwen, A. S., L. Keszthelyi, P. Geissler, D. P. Simonelli, M. H. Carr, T. V. Johnson, K. P. Klassen, H. H. Breneman, T. J. Jones, J. M. Kaufman, K. P. Magee, D. A. Senske, M. J. S. Belton, and G. Schubert 1998a. Active volcanism on Io as seen by Galileo SSI. *Icarus* **135**, 181–219.

McEwen, A. S., L. Keszthelyi, J. R. Spencer, D. L. Matson, R. Lopes-Gautier, K. P. Klassen, T. V. Johnson, J. W. Head, P. Geissler, S. Fagents, A. G. Davies, M. H. Carr, H. H. Breneman, and M. J. S. Belton 1998b. Very high-temperature volcanism on Jupiter's moon Io. *Science* **281**, 87–90.

McEwen, A. S., D. P. Simonelli, D. R. Senske, K. P. Klassen, L. Keszthelyi, T. V. Johnson, P. E. Geissler, M. H. Carr, and M. S. J. Belton 1997. High temperature hot spots on Io as seen by the Galileo Solid-State Imaging experiment. *Geophys. Res. Lett.* **24**, 2443–2446.

Nash, D. B. 1993. A case for Na_2S on Io's surface: Sulfide volcanism? In *Io: An International Conference, San Juan Capistrano, CA*, pp. 75–76.

Nash, D. B., M. H. Carr, J. Gradie, D. M. Hunten, and C. F. Yoder 1986. Io. In *Satellites* (J. A. Burns and M. S. Matthews, Eds.), pp. 629–688. Univ. of Arizona Press, Tucson.

Peale, S. J., P. Cassen, and R. T. Reynolds 1979. Melting of Io by tidal dissipation. *Science* **203**, 892–894.

Pearl, J. C., and W. M. Sinton 1982. Hot spots on Io. In *Satellites of Jupiter* (D. Morrison, Ed.), pp. 724–755. Univ. Arizona Press, Tucson.

Pieri, D. C., S. M. Baloga, R. M. Nelson, and C. Sagan 1984. Sulfur flows of Ra Patera, Io. *Icarus* **60**, 685–700.

Sagan, C. 1979. Sulphur flows on Io. *Nature* **280**, 750–753.

Shoemaker, E. M. 1994. Update on the impact rates in the jovian system. In *Icy Galilean Satellites Conference, San Juan Capistrano Conference*, No. 4. February 1994, p. 77.

Sinton, W. M. 1981. The thermal emission spectrum of Io and a determination of the heat flux from its hot spots. *J. Geophys. Res.* **86**, 3122–3128.

Soderblom T. Johnson, D. Morrison, E. Danielson, B. Smith, J. Veverka, A. Cook, C. Sagan, P. Kupferman, D. Pieri, J. Mosher, C. Avis, J. Gradie, and T. Clarey 1980. Spectrophotometry of Io: Preliminary Voyager 1 Results. *Geophys. Res. Lett.* **7**, 963–966.

Smith, B. A., and the Voyager Imaging Team 1979. The Jupiter system through the eyes of Voyager 1. *Science* **204**, 951–972.

Smythe, W. D., R. M. Nelson, and D. B. Nash 1979. Spectral evidence for SO_2 frost or adsorbate on Io's surface. *Nature* **280**, 766–767.

Smythe, W. D., and 14 colleagues 1995. Galilean satellite observation plans for the Near-Infrared Mapping Spectrometer on the Galileo spacecraft. *J. Geophys. Res.* **100**, 18,957–18,972.

Spencer, J. R., J. A. Stansberry, C. Dumas, D. Vakil, R. Pregler, M. Hicks, and K. Hege 1997. A history of high-temperature Io volcanism: February 1995 to May 1997. *Geophys. Res. Lett.* **24**, 2451–2454.

Stansberry, J. A., J. R. Spencer, R. R. Howell, C. Dumas, and D. Vakil 1997. Violent silicate volcanism on Io in 1996. *Geophys. Res. Lett.* **24**, 2455–2458.

Strom, R. G., N. M. Schneider, R. J. Terrile, A. F. Cook, and C. Hansen 1981. Volcanic eruptions on Io. *J. Geophys. Res.* **86**, 8593–8620.

Thordarson, Th., and S. Self 1993. The Laki (Skaftar Fires) and Grimsvotn eruptions in 1783–1785. *Bull. Volcanol.* **55**, 233–263.

Veeder, G. J., D. L. Matson, T. V. Johnson, D. L. Blaney, and J. D. Goguen 1994. Io's heat flow from infrared radiometry: 1983–1993. *J. Geophys. Res.* **99**, 17095–17162.

Witteborn, F. C., J. C. Bregman, and J. B. Pollack 1979. Io: An intense brightening near 5 micrometers. *Science* **203**, 643–646.

Zahnle, K., L. Dones, and H. F. Levison 1998. Cratering rates on the Galilean Satellites. *Icarus* **136**, 202–222.